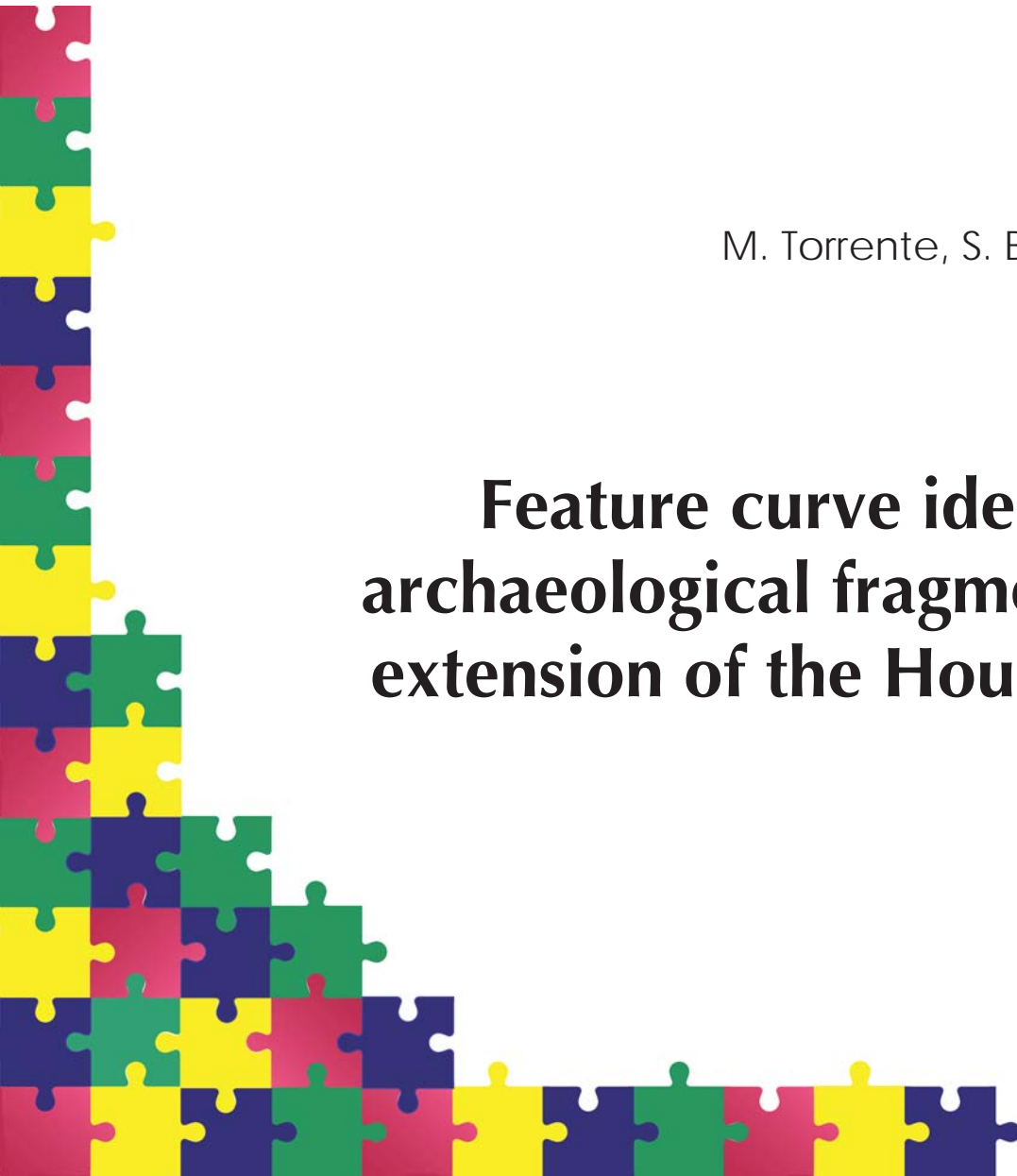


REPORT SERIES

M. Torrente, S. Biasotti, B. Falcidieno

Feature curve identification in archaeological fragments using an extension of the Hough transform



IMATI REPORT Series

Nr. 16-09 – July 2016

Managing Editor

Paola Pietra

Editorial Office

Istituto di Matematica Applicata e Tecnologie Informatiche “E. Magenes”

Consiglio Nazionale delle Ricerche

Via Ferrata, 5/a

27100 PAVIA (Italy)

Email: reports@imati.cnr.it

<http://www.imati.cnr.it>

Follow this and additional works at: <http://www.imati.cnr.it/reports>

Copyright © CNR-IMATI, 2016.

IMATI-CNR publishes this report under the Creative Commons Attributions 4.0 license.

**Feature curve identification in archaeological
fragments using an extension of the Hough
transform**

M. Torrente, S. Biasotti, B. Falcidieno

Abstract.

The use of computer graphics techniques in cultural heritage (CH) has led to impressive improvements in technologies related to digital acquisition and rendering of 3D CH data. Digitized artefacts are becoming widely available for access and reuse, thus increasing the need of tools able to support comparative shape analysis. As 3D artefacts are often worn, eroded and broken, these tools cannot take advantage of existing methods based on exact matching but they rather require new approaches able to identify partial features in portions of models thus leading to a double partiality of the matching problem, in terms of both features and models. In this context, we propose a method based on a novel generalization of the Hough transform technique able to identify and localize semantic features like anatomical features, ornaments, or decorations on digital artefacts or fragments, even if the features are partially damaged or incomplete. The major advantages of using a method based on the Hough transform technique are the relative robustness to noise and the recognition power also in the case of partial features. Our experiments on digital models of real artefacts are encouraging and show the potential of the method, which can work on both 3D meshes and point clouds.

Keywords: *Future identification, Hough transform, Cultural heritage*

Corresponding author: Silvia Biasotti - IMATI-CNR, Genova - email: silvia@ge.imati.cnr.it

Feature curve identification in archaeological fragments using an extension of the Hough transform

M. Torrente, S. Biasotti, B. Falcidieno

July 14, 2016

Abstract

The use of computer graphics techniques in cultural heritage (CH) has led to impressive improvements in technologies related to digital acquisition and rendering of 3D CH data. Digitized artefacts are becoming widely available for access and reuse, thus increasing the need of tools able to support comparative shape analysis. As 3D artefacts are often worn, eroded and broken, these tools cannot take advantage of existing methods based on exact matching but they rather require new approaches able to identify partial features in portions of models thus leading to a double partiality of the matching problem, in terms of both features and models. In this context, we propose a method based on a novel generalization of the Hough transform technique able to identify and localize semantic features like anatomical features, ornaments, or decorations on digital artefacts or fragments, even if the features are partially damaged or incomplete. The major advantages of using a method based on the Hough transform technique are the relative robustness to noise and the recognition power also in the case of partial features. Our experiments on digital models of real artefacts are encouraging and show the potential of the method, which can work on both 3D meshes and point clouds.

1 Introduction

The use of 3D computer graphics techniques in cultural heritage (CH) has led to impressive improvements in technologies related to digital acquisition and rendering of 3D CH data. A new generation of 3D scanners and digital photography devices has made possible to capture not only a highly detailed 3D geometry of artefacts, but also textures and optical material properties [SWRK11, SRT*14]. Also rendering tools provide digital reproductions that cannot be distinguished from pictures of the real objects captured with a real camera and 3D printers can fabricate accurate physical copies, which replace traditional reproductions.

Making cultural artefacts digitized and widely available for access and reuse is now becoming a reality, as hypothesized in the EU report *New Renaissance* [NDL11] and 3D repositories containing the digital surrogates of artefacts or fragments together with technical metadata are becoming commonplace [STA, Ham]. Archaeologists can explore cultural artefacts, both complete objects and fragments, without manipulating them physically and even if sparse in different museums or collections. These achievements open new perspectives to a new generation of professionals in the CH domain (curators, conservators, researchers), they give them significant benefits by allowing

a ubiquitous access to information from a variety of heterogeneous data sources and supporting the investigation of findings with other colleagues of different cultural, historical and geographic context.

While in the earlier times of 3D computer modelling application in the CH domain mainly the object's geometry and appearance were in the centre of interest, now archaeologists are asking that 3D models become a valuable source to support activities of comparative analysis [PPY*16]. Some of them are related to *re-unification* tasks, e.g. to select fragments belonging to the same archaeological type or to find matching between fragments for reassembly purposes. Other activities are related to *re-association* purposes, to classify objects according to various criteria, e.g., geometric shapes, textures or semantic features. What is crucial in these tasks is to have at disposal computer models and tools useful to compare objects and fragments, identify features, filter noise and degradation, record and model semantic data.

However, several problems make these tasks very complex to be solved. Archaeological artefacts are often broken, eroded, worn, or incomplete and their quantity is extremely vast, distributed and fragmented. Archaeologists have to hypothesize a dynamic and unseen past world interpreting partial and inanimate remains of it and to face with the intrinsic uncertainty of what data represent and the variety of possible valid descriptions.

Therefore, the nature of archaeological data calls for methods dealing with multi-modal information in combination (e.g., geometry, pattern, texture, colour, reflectance). For this reason, there is an increasing number of techniques that complement the geometric analysis with pattern/colour information, for instance to disambiguate fragments re-assembly [WC08, ASC*13, KDS10], or to virtually match them [BCFS15].

A further complexity is that global similarity is often not applicable in the CH domain, as many artefacts are found broken and eroded. In general, the goal is to detect similar parts on other surfaces, regardless of the global surface this part belongs to [LBZ*13]. Recently, some methods for partial similarity evaluation of artefacts have been devised for specific tasks, such as the retrieval of partially broken pottery in [SPS15], or looking for complete sub-parts, such as the recognition of object reliefs or coin stamps [IT11]. Unfortunately, this is not enough general in a broader context. Indeed, when dealing with broken fragments, a further challenge is to identify, and locate, partial features in portions of models (for instance, a broken eye in a part of a head), thus leading to a *double partiality* of the matching problem, in terms of both features and models.

Another consideration is that the description of an artefact is usually a text often integrated with pictures or manual sketches, but completely unrelated to its digital model. Therefore its semantic features are recognizable or localizable in the 3D model only through visualization, while they should be attributed to it.

In this paper we propose a method to identify and localize semantic features like anatomical features, ornaments or decorations on the digital models of archaeological artefacts or their fragments, even if the features are partially damaged or incomplete. The focus of our contribution is on the extraction of feature curves from a set of potentially significant points using an extension of the Hough transform technique for their approximation, producing a family of primitive curves that are flexible to meet the user's needs. The method allows the recognition of various features, possibly compound, and the selection of the most suitable profile among the family of algebraic curves. The major advantages of using a method based on the Hough transform are the relative robustness to noise and the recognition power also in the case of partial features. Our experiments on digital artefacts are encouraging and show the potential

of the method, which can work on both 3D meshes and point clouds.

The remainder of the paper is organized as follows. In Section 2, we describe previous work on the extraction of feature curves and an introduction to the Hough transform technique. In Section 3 we explain the steps for extracting peculiar curves from feature points. Experimental results are shown and commented in Section 4 and Section 5 concludes the paper.

2 Previous work on feature curves extraction

In computer graphics the extraction of salient features from surfaces or point clouds has been addressed either in terms of lines [GWM01], shape segments [Sha06] and descriptions [BDF*08]. In the case of artefacts, feature curves have been shown to be quite a flexible choice for representing the salient parts of the model [KIST11, HT11].

A popular choice to locate where the feature curves lie is to estimate the curvature, either on meshes [YBYS08, KST08] or point clouds [GWM01, DIOHS08]. Feature lines are often characterized as ridges and valleys, thus representing the extrema of principal curvatures [OBS04, YBYS08]. Curvature is often approximated with fitting methods, either global [OBS04] or local [YBYS08, KK06]. Among the others, the authors in [KK06] incorporate also colorimetric information addressing the fitting problem in a six-dimensional space. An alternative approach to locate curvature extrema is to use discrete differential operators [HPW05] or probabilistic methods, such as random walks [LLZ10]. When dealing with curvature estimation, parameters have to be tuned according to the target feature scale and the underlying noise. In general, approaches based on the Moving Least Square method [PKG03] and its variations are robust to different scale [DIOHS08] and do not incorporate smoothness effects in the estimation.

Other types of lines used for feature curve representation are parabolic. They partition the surface into hyperbolic and elliptic regions, and zero-mean curvature curves, which classify sub-surfaces into concave and convex shapes [Koe84]. Parabolic lines correspond to the zeros of the Gaussian and mean curvature, respectively. Finally, demarcating curves are the zero-crossings of the curvature in the curvature gradient direction [KST08, KIST11].

Recently, [APM15] used feature curves to drive fragment reassembly. In their work, a local estimation method is initially adopted to compute the mean curvature at each vertex of a mesh using seven scales. Then, salient points are grouped in a curve skeleton. Finally, user's interaction is needed to select the group of points to be fitted with a quadratic spline approximation.

Besides the most popular quadratic splines, the set of curves candidates to fit a feature line is very large, for instance recently 3D Euler spiral has been proposed as a natural way to describe line drawing and silhouettes showing its suitability for shape completion [HT11].

In this sense, our approach follows well established paradigms of characterizing feature points as curvature or colour extrema but differs from the previous literature for the novel introduction of an extension of the Hough transform in the 3D domain. This technique is a standard pattern recognition method to detect profiles in images using algebraic curves. We briefly explain the method's main idea starting from its original use (see [Hou62], [DH72]). Let $y - ax - b = 0$ (with a, b independent real parameters) be the equation of a family of straight lines and let $p = (x_p, y_p)$ be a point in the image plane. The Hough transform (HT) of p is the straight line of equation

$ax_p + b - y_p = 0$ in the parameter plane (the equation now reads in the indeterminates a, b). Fix now a line l of equation $y - Ax - B = 0$ (with A, B real values); the usual point-line duality of projective plane implies that all points p_j of l have as Hough transform lines in the parameter plane intersecting at the unique point (A, B) , which therefore can be used to unambiguously identify the original line $l : y - Ax - B = 0$. In the real-world cases, points in the image space appearing as visually aligned are actually almost aligned (due to noise, to the pixel dimensions, and so on) and this translates to a “cluster” of crossings of the Hough transforms in the parameter space. In order to get the instance of the family of lines which best approximates the almost aligned points, (a region of) the parameter space is discretized and a histogram (usually called *accumulator function*) counting the number of crossings is constructed on it. In the parameter space the discretization cell corresponding to the maximum of the accumulator function identifies the parameters values of the line best approximating the given profile.

Since its original conception, the Hough transform has been extensively used and many generalizations have been proposed for identifying positions of arbitrary shapes, most commonly circles or ellipses [Bal81]. More recently, the Hough transform technique has been extended and applied to different families of algebraic curves (see [BR12] and [BMP13]). This is undoubtedly an advantage of the method, which allows to deal with various shapes, possibly compound, and to choose the most suitable approximating profile among a broad vocabulary of curves. Another important advantage of the Hough transform method stands in its relative robustness to noise.

3 Selection of curves from feature points

In this section we provide a detailed description of the method that we propose for extracting peculiar curves from feature points of a given 3D model. To show the characteristics of the method, we have applied it to the analysis of statue’s fragments, focusing on some anatomical features usually highlighted by the curator in the free form text notes (such as eyes and mouth), but the method is general and could be applied to other cases (other anatomical features, extraction of patterns, localization of decorations).

We assume that the geometric model of the object is available as a triangulated mesh with colour, since, nowadays, many sensors are able to acquire not only the geometry of an object but also its colours. Nevertheless, these working assumptions are not fully needed by our methodology and can be weakened. The model’s photometric features, which, if present, contain rich information about the real appearance of objects (see [TWW01]), can be exploited alone or in combination with the shape properties for extracting the feature points set. However, if the model has no colour, only the geometrical information will be used. Further, our methodology does not require any regularity of the triangulated mesh. Good properties (like watertightness) are needed requirements of the used software (see Section 3.1), though in principle our approach is able to handle even simple point clouds. To this end, in our experiments (see Section 4), when dealing with non optimal meshes or point clouds, a preprocessing step will be adopted.

The methodology, described in Section 3.1-3.4 also through an illustrative example, consists of 4 stages that permit us to apply the Hough transform to points instead of images. First, the feature points are characterized by means of geometric and/or photometric descriptors (Section 3.1). Then, the selected vertices are divided into smaller connected components (Section 3.2). The next two steps apply to each computed com-

ponent: each subset is projected onto its best fit plane (Section 3.3) and a feature curve is automatically associated, via the HT-based technique, to the 2-dimensional set of feature points (Section 3.4).

3.1 Feature point characterization

In the general case, when a 3D model with colour is available, we propose a shape analysis able to extract both geometric and photometric information. The geometric properties can be easily derived using classical curvature functions, like minimum, maximum or mean curvatures. Curvature quantities are computed and displayed using the Matlab Toolbox Graph [Pey]. The photometric properties can be represented in different colour spaces, such as RGB, HSV, and CIELab spaces. Our choice is to work in the CIELab space [AKK00], which has been proved to approximate human vision in a good way. In such space, tones and colours are kept distinct: the L channel is used for the luminosity which closely matches the human perception of light ($L = 0$ yields black and $L = 100$ yields diffuse white), whereas the a and b channels specify colours, from magenta to green (negative values of a indicate magenta, positive values of a indicate green) and from yellow to blue (negative values of b indicate yellow, positive values of b indicate blue). The curvature (C_{min} is the minimum curvature, C_{max} the maximum curvature, C_{mean} the mean curvature and C_{Gauss} the Gaussian curvature) and the luminosity L are used, separately, as scalar real functions, and denoted by $f_{C_{min}}$, $f_{C_{max}}$, $f_{C_{mean}}$, $f_{C_{Gauss}}$, f_L respectively. In this section, as illustrative example we use a 3D model \mathcal{M} derived from a scanned artefact of the STARC repository [STA] (see Figure 1).



Figure 1: A Salamis terracotta fragment, [STA].

The model \mathcal{M} is given as a triangulated mesh (with colour). A representation of the main curvature functions computed on the model \mathcal{M} is shown in Figure 2 (a)-(d).

The feature points \mathbb{X} of the model \mathcal{M} are extracted by selecting the regions at which these functions assume particular values (e.g high maximal curvature and/or low minimal curvature and/or low luminosity) and this is achieved by simply using their histograms (see Figure 3).

In particular, in our illustrative example the set \mathbb{X} of feature points is obtained by selecting the vertices of the model \mathcal{M} having low luminosity (smaller than 30%) and low minimum curvature (smaller than 30%) or high maximum curvature (bigger than 65%), see Figure 4.

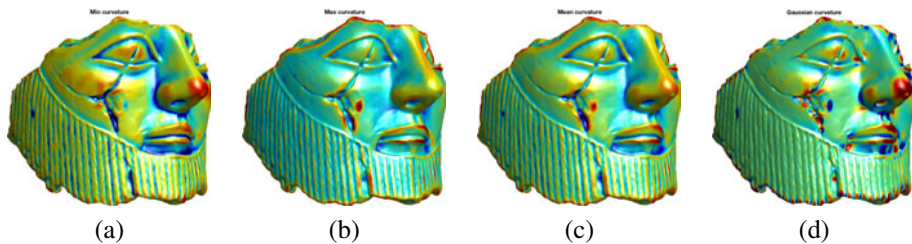


Figure 2: Values of curvature functions on the model \mathcal{M} : (a) minimum curvature, (b) maximum curvature, (c) mean curvature, (d) Gaussian curvature.

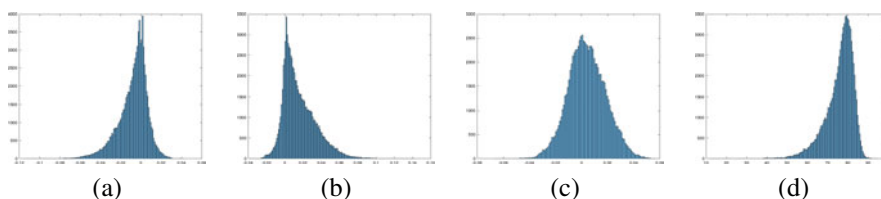


Figure 3: Histograms of: (a) minimum curvature values $f_{C_{min}}(\mathcal{M})$, (b) maximum curvature values $f_{C_{max}}(\mathcal{M})$, (c) mean curvature values $f_{C_{mean}}(\mathcal{M})$, (d) luminosity values $f_L(\mathcal{M})$.

3.2 Clustering

To highlight the anatomical features of the model \mathcal{M} , the set \mathbb{X} of feature points is partitioned into smaller connected components using the DBSCAN (Density-Based Spatial Clustering of Applications with Noise) method [EKSX96]. DBSCAN is an algorithm designed to efficiently identify clusters of arbitrary shapes. It relies on a density-based notion of clusters and noise: the main idea is that each point of a cluster must be surrounded (within a certain distance) by a minimum number of neighbours, that is, the density in the neighborhood has to exceed some given threshold. The points that do not satisfy these requirements (i.e. lying in low-density regions) are regarded as noise. DBSCAN requires two parameters: a real positive number ϵ , which is the threshold used as the radius of the density region, and a positive integer i , which is the minimum number of points required to form a dense region. In order to relate the choice of the threshold ϵ to the context, we use the function *knnsearch* of MATLAB. This function, based on the algorithm described in [FBF77], finds the k nearest neighbours of each point of a given dataset. Using it, we can have a clue of the spatial distribution of the feature points belonging to \mathbb{X} , and consequently fix the value of ϵ . Figure 5 shows an example of the use of DBSCAN (with $\epsilon = 0.2608$, the average of the distance of the 20th nearest points, and $i = 5$) on the feature points \mathbb{X} represented in Figure 4. The set \mathbb{X} has been partitioned into 60 clusters (corresponding to different colours, see Figure 5 (a)) and a collection of outliers (see Figure 5 (b)).

3.3 Point cloud projection

This step reduces the problem from the 3-dimensional to the 2-dimensional case. This operation is not a restriction of our method, but derives from the fact that the features

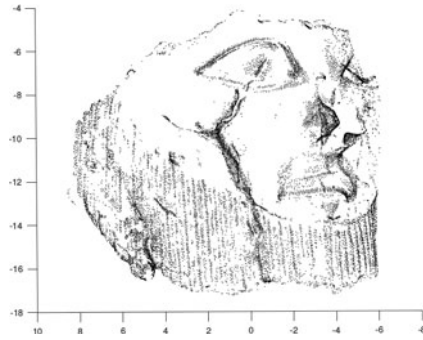


Figure 4: Set \mathbb{X} of feature points obtained by selecting the vertices of \mathcal{M} having low luminosity (smaller than 30%) and low minimum curvature (smaller than 30%) or high maximum curvature (bigger than 65%).

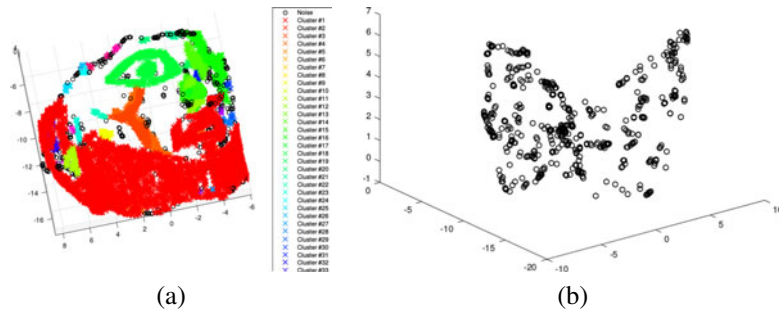


Figure 5: Partition of the point set \mathbb{X} into (a) 60 coloured clusters and (b) noisy points (in black), applying DBSCAN to \mathbb{X} with parameters $\epsilon = 0.2608$ and $i = 5$.

contour lines which we are interested to extract (like eyes and mouth) locally present a well identifiable shape mostly defined by planar curves. The points of each component \mathbb{X}_i resulting from the clustering step (as described in Section 3.2) are processed as follows: a translation is applied to move the centroid of the points of \mathbb{X}_i onto the origin. Then, a best fitting plane Π_i for the points of \mathbb{X}_i is found by computing the multiple linear regression using least squares. We apply a *regression* function to the matrix X of size $s \times 2$ and the vector Y of size $s \times 1$, where s is the number of points, which are built as follows. The two columns of the matrix X contain the x - and y -coordinates of the points of \mathbb{X}_i , whereas Y contains the z -coordinates of the points. Thus, the best fitting plane Π_i has equation $\Pi_i : z - B_1x - B_2y = 0$. Then, the points of \mathbb{X}_i are orthogonally projected on Π_i forming the new points set \mathbb{Y}_i . Finally, the orthogonal transformation φ_i moving the plane Π_i onto the plane $z = 0$ is defined and applied to points set \mathbb{Y}_i to get the new set \mathbb{Z}_i . Figures 6 (a)-(b) show the output of the whole procedure on the cluster \mathbb{X}_{22} (coloured in green in Figure 5 (a)); in particular, Figure 6 (b) represents the set of points \mathbb{Z}_{22} (in black).

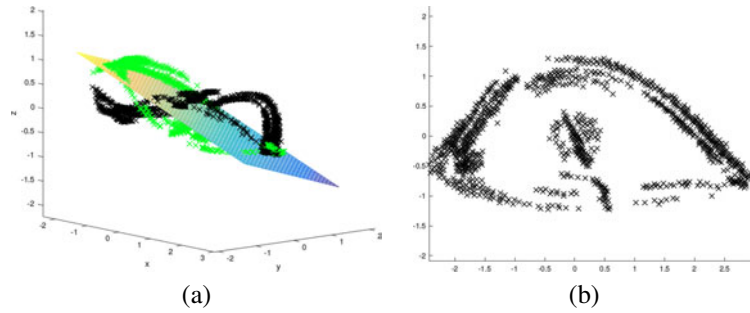


Figure 6: The procedure of point cloud projection applied to a cluster set: (a) the set \mathbb{X}_{22} (in green), its best fitting plane and the point set projection \mathbb{Z}_{22} (in black); (b) the set of points \mathbb{Z}_{22} .

3.4 From points to feature curves

To automatically detect feature curves from a selected set of points, we apply a generalization of the Hough transform technique (see [BMP13], [MPCB15], [TB14]). With respect to the previous literature on images, the application of the Hough transform to the projected 3D points is novel and do not undergo to grid approximation of the coordinates of the points. One advantage of this method is the flexible choice of the family of algebraic curves used to approximate the desired features, thus being adaptive to approximate various shapes. In our “vocabulary” the set of primitives includes many algebraic curves in addition to the more common ones, like straight lines, circles, ellipses, parabolic lines, etc.

For example, in the case of an eye feature, one interesting family of algebraic curves is the so-called *geometric petal* [Shi95] whose shape resembles, for particular values of the parameters, the eye contour line. Its polar equation is:

$$\rho = a + b \cos^{2n} \theta$$

with n integer and a, b real numbers. The geometrical petal is a bounded symmetric curve with a singularity at the origin. Some examples are provided in Figure 7 where the values of the parameters are set as follows: $a = 2$, $b = -2$ and $n = 1, 10, 50, 100$.

For our purposes, we can restrict to the case $b = -a$. In this case, we observe that the curve is completely contained inside the circle of radius $\sqrt{2a}$. We pass to the cartesian equation using the standard substitutions $\rho = \sqrt{x^2 + y^2}$ and $\cos \theta = x / \sqrt{x^2 + y^2}$; further, in order to lower the parameters degree, we replace a by \sqrt{a} . The cartesian equation of the geometric petal is $g_a(x, y) = 0$ where

$$g_a(x, y) = (x^2 + y^2)^{2n+1} - a[(x^2 + y^2)^n - x^{2n}]^2$$

Most of the times for the extraction/localization of eyes we need a shape which is more stretched along the x -axis (see Figure 8). We can stretch the geometric petal by scaling the x -variable by a factor of \sqrt{c} , where c is a positive real parameter. The new cartesian equation of the curve is $g_{a,c}(x, y) = 0$ where

$$g_{a,c}(x, y) = (cx^2 + y^2)^{2n+1} - a[(cx^2 + y^2)^n - c^n x^{2n}]^2$$

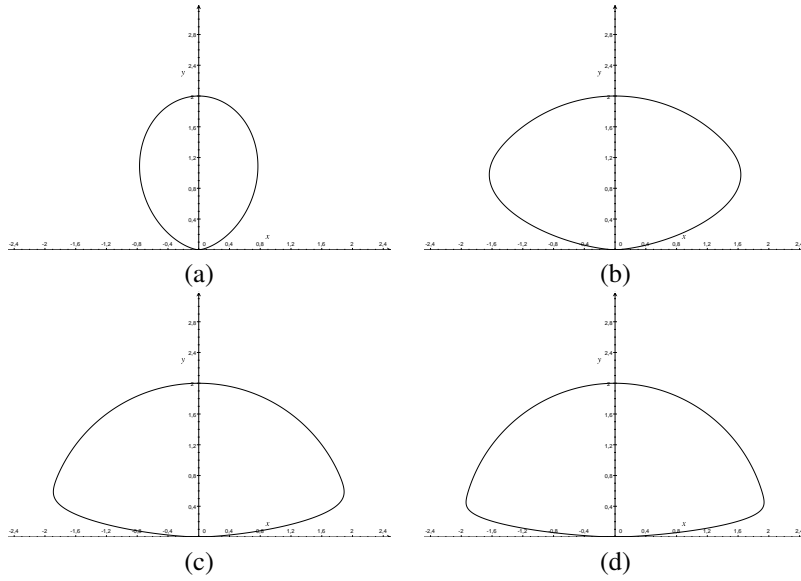


Figure 7: Geometric petal curve with $a = 2$, $b = -2$ and: (a) $n = 1$, (b) $n = 10$, (c) $n = 50$, (d) $n = 100$.

Some observations on the geometry of the geometric petal curve allow us to recover the value of the exponent parameter n , which has to satisfy the following condition:

$$\frac{2n}{2n+1} \left(1 - \sqrt[n]{\frac{1}{2n+1}} \right)^{1/2} = \frac{y_B}{y_A}$$

where y_A and y_B are the y -coordinates values of the points A and B (see Figure 8). Applying the previous considerations and the HT-based procedure to the family $g_{a,c}(x,y) = 0$ and the set \mathbb{Z}_{22} (see Figure 6 (b)), we get a curve defined by parameter values $n = 78$, $a = 6.4168$ and $c = 0.8162$ (see Figure 9 (a)).

If we are looking for a mouth feature, another interesting shape is given by the sextic surface of equation

$$a^4(x^2 + z^2) + (y - a)^3 y^2 = 0$$

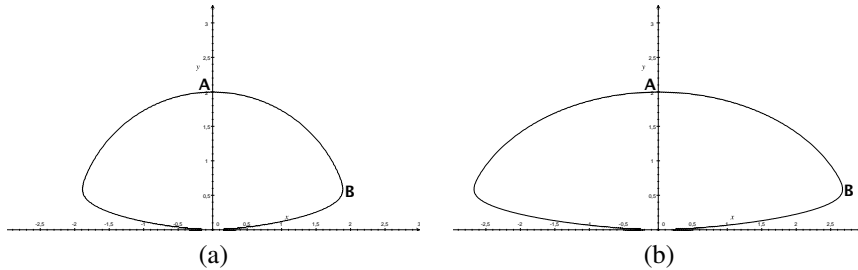


Figure 8: Geometric petal curve defined by $g_{a,c}(x,y) = 0$ with $a = 4$, $n = 50$ and: (a) $c = 1$, (b) $c = 1/2$.

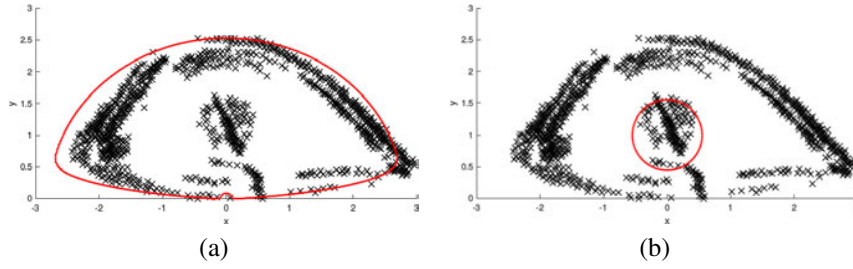


Figure 9: Point set \mathbb{Z}_{22} and (a) the geometric petal curve (in red) of equation $g_{a,c}(x,y) = 0$ with parameters $n = 78$, $a = 6.4168$ and $c = 0.8162$, (b) the circumference centered at $(0, 1)$ with radius $11/20$.

with a real parameter, called the *zitrus* (or *citrus*) *surface* by Herwig Hauser [Ima].

The citrus surface has bounding box $((-\frac{a}{8}, \frac{a}{8}), (0, a), (-\frac{a}{8}, \frac{a}{8}))$, centroid at $(0, \frac{a}{2}, 0)$ and volume $\frac{1}{140}\pi a^3$. We are interested in an orthogonal section of the citrus surface (cutting with the plane $x = 0$ or $z = 0$). Applying a rotation of $\pi/2$ and centering the curve at the origin we obtain the *citrus curve* of equation $f_a(x,y) = 0$ where $f_a(x,y)$ is the following sextic polynomial

$$f_a(x,y) = a^4 y^2 + \left(x - \frac{a}{2}\right)^3 \left(x + \frac{a}{2}\right)^3$$

with a real number (see Figure 10 (a)). The citrus curve is a symmetric bounded curve with bounding box $((-\frac{a}{2}, \frac{a}{2}), ((-\frac{a}{8}, \frac{a}{8}))$.

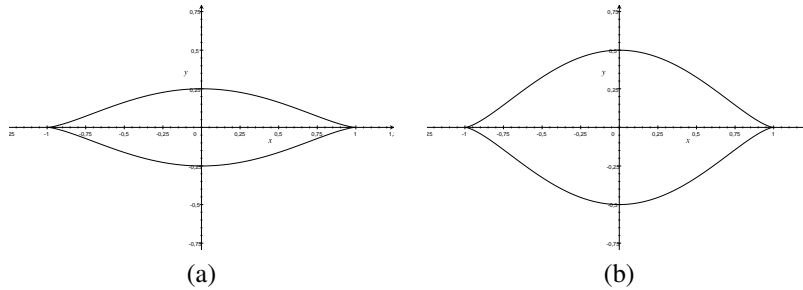


Figure 10: The citrus curve of equation: (a) $f_a(x,y) = 0$ with $a = 2$, (b) $f_{a,c}(x,y) = 0$ with $a = 2$, $c = 1/2$.

Most of the times for the localization of eyes and/or mouth we need a shape which has a different ratio. To this aim, we introduce another citrus curve whose equation is $f_{a,c}(x,y) = 0$ (which is simply stretched or shortened along the y -axis) where $f_{a,c}(x,y)$ is given by:

$$f(x,y) = a^4 c^2 y^2 + \left(x - \frac{a}{2}\right)^3 \left(x + \frac{a}{2}\right)^3$$

with a, c real numbers (see Figure 10 (b)). Note that this is again a symmetric bounded curve with bounding box $((-\frac{a}{2}, \frac{a}{2}), ((-\frac{a}{8c}, \frac{a}{8c}))$.

Other more obvious but likewise interesting families of algebraic curves are ellipses, circles and straight lines, which can be exploited to detect for instance eyes contours, pupils shapes and lips lines. Their equation are quadratic (ellipses and circles) and linear (straight lines) and depend on 3 parameters at most. Applying the HT-based procedure to the generic family of circumferences and the set \mathbb{Z}_{22} (see Figure 6(b)), we get the curve of equation $(x + 2/25)^2 + (y - 2/25)^2 - (11/20)^2 = 0$ (see Figure 9(b)).

To grasp compound shapes, it is possible to use different curves. For instance, to extract the eye shape in its entirety we can detect a circumference and successively a geometric petal curve (see Figure 11 (a)), taking advantage of the circumference's position and dimension for restricting the parameters space of the geometric petal curve. Another approach is to define a more structured family of algebraic curves starting

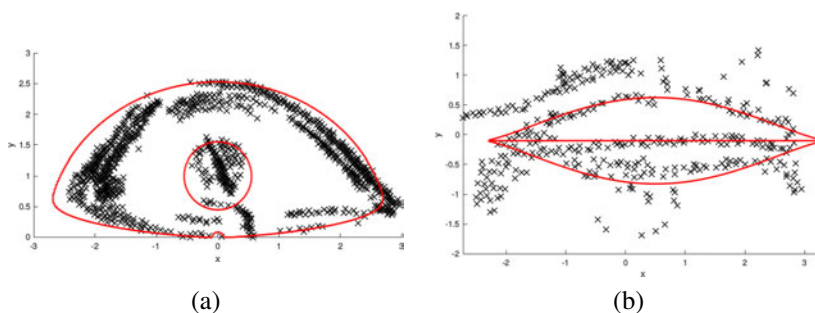


Figure 11: Combined shapes: (a) a circumference and a geometric petal curve detecting an eye; (b) a citrus curve with a line detecting a mouth.

from two or more simple families. This is the case of the mouth contour which can be detected combining a citrus curve with a line: to this aim we introduce the family of algebraic curves defined by $h_{a,c}(x,y) = 0$ where:

$$h_{a,c} = y(a^4 c^2 y^2 + \left(x - \frac{a}{2}\right)^3 \left(x + \frac{a}{2}\right)^3).$$

An example of this detection is represented in Figure 11(b). This second approach has the clear advantage of simultaneously detecting compound features with the inconvenience of handling more complex families of algebraic curves (that is, defined by higher degree polynomials).

4 Experimental results

The proposed methodology has been tested on a collection of artefacts collected from the STARC repository [STA] and the AIM@SHAPE repository [EC15]. Figure 12 contains images of the chosen models: the models of cases A and B are taken from [EC15], whereas the models of cases C, D, E and F are taken from [STA].

All the models, except model D, are available as triangulated meshes; model D is given as a point cloud set. In the cases A, B and C the colour is not available, so only the geometrical information (via maximum and minimum curvature functions) is used to extract the feature points set. In the remaining cases the geometry is combined with the chromatic information. In all the cases, the models position inside the 3-dimensional space is completely random and a "best" view is artificially reported in Figure 12,

columns 1 and 2, for reader’s convenience. Further, to lower the computational costs, the number of vertices of the models original meshes is reduced using the MeshLab function *Quadric Edge Collapse (with texture)* [Vis].

Experiments represented in Figure 12 are aimed to the extraction of eyes. The parameters’ values of the detected curves are gathered into three tables: Table 1 contains the parameters of the citrus curves, Table 2 contains the centers and the radii of the circumferences, and Table 3 contains the degree and the parameters of the geometric petal curves.

Model	a	c
A - right eye	31	0.23
A - left eye	30	0.23

Table 1: Parameters of detected citrus curves.

Model	radius
A - right eye	3.633
A - left eye	3.661
E - right eye	0.283
E - left eye	0.3

Table 2: Radius of detected circumferences.

Model	n	a	c
B - right eye	50	308.25	1.4484
B - left eye	50	245	0.7503
C - right eye	45	1115	0.6738
C - left eye	45	993	0.7334
D - right eye	75	3.12	0.5855
D - left eye	75	3.05	0.8306
E - right eye	75	1.08	0.6675
F - right eye	75	1.08	0.7141

Table 3: Parameters of detected geometric petal curves.

The contours of the two eyes are independently detected in the cases A-D. The parameters of the detected citrus curves for the model A are very similar for the right and the left eye (see Table 1). As for the detected geometric petal curves, a proper comparison should involve the square roots of the parameters values reported in Table 3, since \sqrt{a} and \sqrt{c} completely mark out the curve (see Section 3.4). An interesting phenomenon is presented by case D: the values of the parameter a are nearly the same, meaning that the two eyes heights are approximately the same, whereas a difference can be noticed in the values of the parameters c , which can be ascribed to the partiality of the left eye. The left and right pupils are visible and independently extracted in the cases A and E: the parameters which makes sense to compare are the circumference radii which are approximately the same in each model (see Table 2). Due to faded colours, in models E and F the left eye contours are difficult to be extracted: the geometric petal curves obtained from the right eyes are used to properly recognize the left eye shape (see Figure 12).

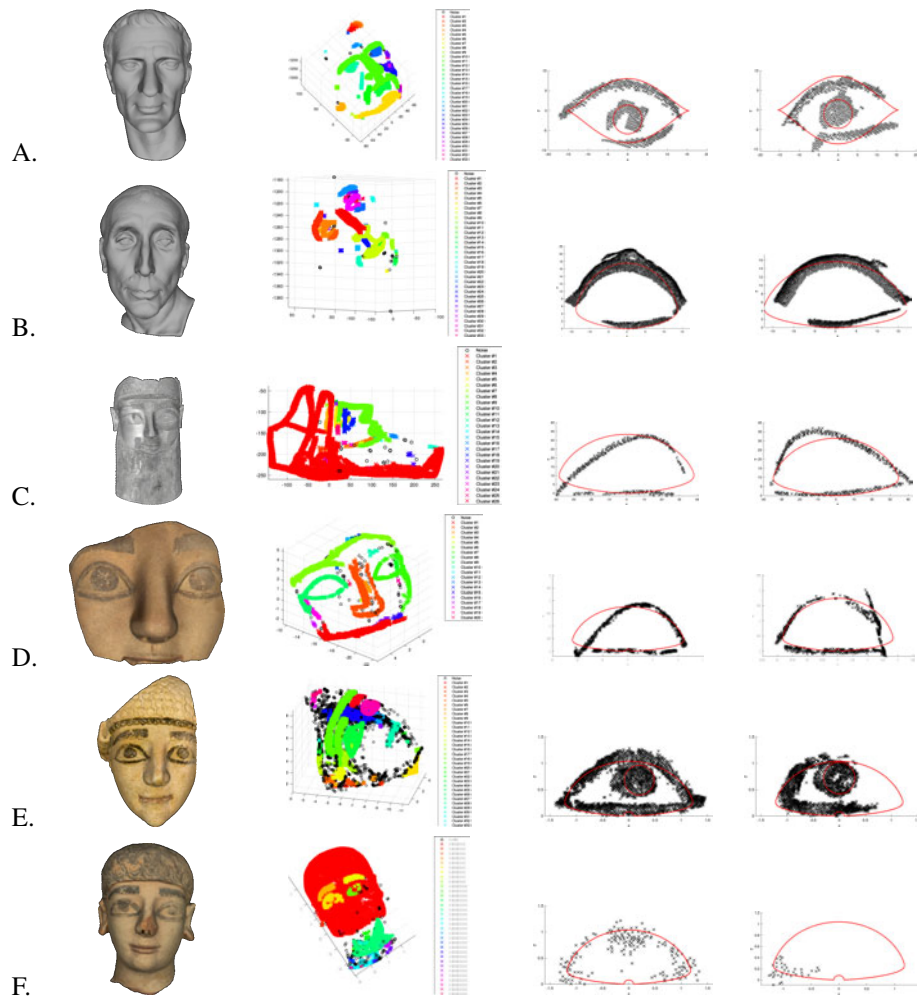


Figure 12: Detection of eye contours and pupils on collection of artefacts collected from the STARC repository [STA] and the AIM@SHAPE repository [EC15].

It is important to point out how close the parameters of the models E and F are, this suggesting that the proposed method could be used to extract the parameters which characterize a style and that may possibly be employed for eyes' detection on other artefacts of the same collection. As for the cases C and D, we observe that the parameters are not comparable to each other neither to those of A and B since the eyes dimensions are not uniformly scaled.

Figure 13 reports experiments on the detection of mouth contours: the first experiment involves model A whose mouth is detected via a geometric petal curve of parameters $n = 50$, $a = 156$ and $c = 0.3444$ (see Figure 13 (a)); in the second experiment model F is considered and its mouth is represented via a citrus curve of parameters $a = 2.15$ and $c = 0.9$ (see Figure 13 (b)).

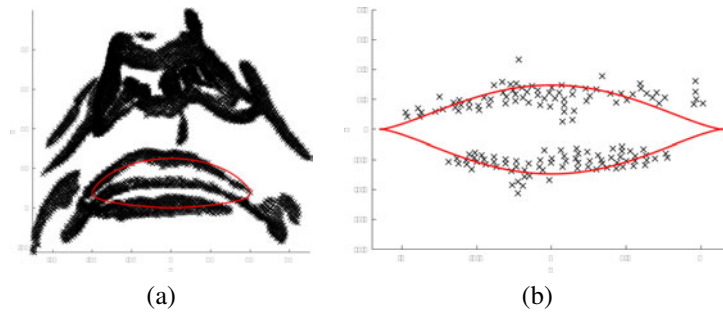


Figure 13: Detection of mouth contours of models A and F of Figure 12: (a) geometric petal curve of parameters $n = 50$, $a = 156$, $c = 0.3444$; (b) citrus curve of parameters $a = 2.3$, $c = 0.95$.

5 Conclusive remarks

This paper presents a novel method to identify features like anatomical characteristics or decorations in digital artefacts or fragments, even if the features are partially damaged or incomplete. We have shown how the method can be applied to fragments arbitrarily embedded in the 3D space and that the only assumption is that the features can be locally projected on a plane. In this way, we have introduced a novel generalization of the Hough transform applied to 3D curves extracted from a set of potentially significant points of the input digital model. In the experiments we mainly focused on the detection of anatomical features because more affected by shape variability and therefore complex with respect to geometric decorations such as the ornaments shown in Figure 15. In this case, the decoration is a repeated pattern of leaves (Figure 15(a,b), each one identified with a specific cluster (Figure 15(c)) and approximated by a citrus curve (Figure 15(d)).

The major advantages of this method are the relative robustness to noise, the recognition power also in the case of partial features and the possibility of working on both 3D meshes and point clouds. In addition, it is important to point out that it similarly parametrizes features that are comparable, see for example the left and right eyes of the head of Figure 12 A, and the eyes of the two heads of Figure 12 E and F. Another interesting point is the possibility of recognizing compound features, as for the eye contour and the pupil.

Furthermore, as we extract a feature pattern and its parameters, we can use them to build a template useful for searching similar features in the artefacts, even if heavily incomplete. This strategy has been used for example to locate the broken eye in the model of the object depicted in Figure 1. Thanks to the identification of the right eye, the geometric petal obtained (Figure 14-(a)) has been used to detect the shape of the damaged left eye (Figure 14-(b)).

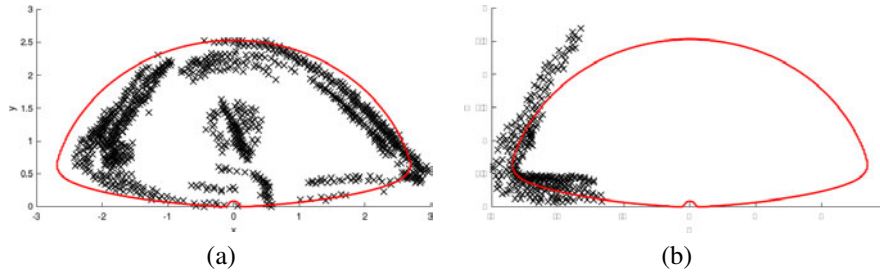


Figure 14: Geometric petal obtained for the right eye (a) used to detect the shape of the damaged left eye (b).

As a minor drawback, we point out that the use of more complex algebraic curves may involve more than three parameters which has consequences in the definition and manipulation of the accumulator function, which becomes computationally expensive, but ad-hoc methods have been introduced to solve it (see [TB14]).

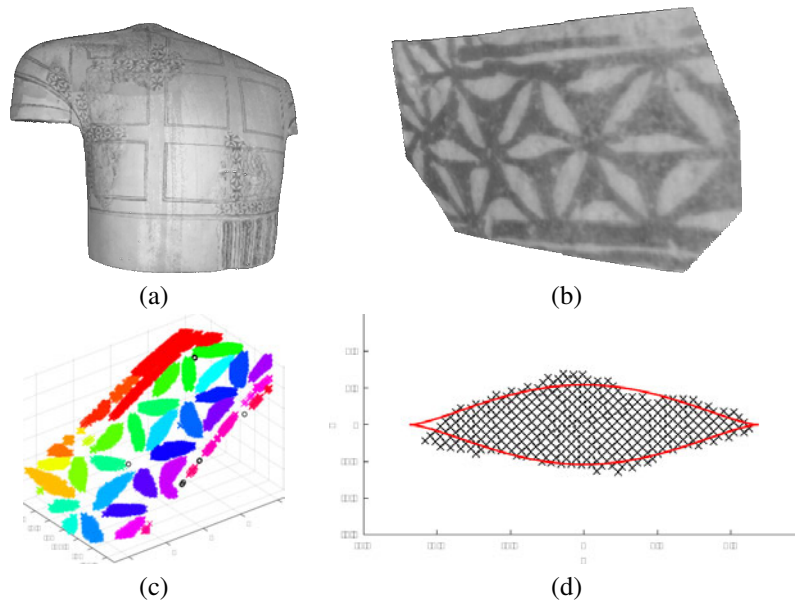


Figure 15: Detection of a decorative pattern on an artefact of the STARC repository [STA]: (a) the original model, (b) a portion of the model, (c) clusters of feature points and (d) detection of an elemental decoration with a citrus curve of parameters $a = 0.95$ and $c = 1.2$.

Acknowledgements Work developed in the CNR research activity ICT.P10.009, and partially supported by GRAVITATE, European project “H2020 REFLECTIVE”, contract n. 665155, (2015-2018). Shapes are courtesy of AIM@SHAPE Repository and the STARC repository [STA].

References

- [AKK00] ALBUZ E., KOCALAR E. D., KHOKHAR A. A.: Quantized cielab* space and encoded spatial structure for scalable indexing of large color image archives. In *Acoustics, Speech, and Signal Processing, ICASSP '00* (2000), vol. 6, pp. 1995–1998.
- [APM15] ANDREADIS A., PAPAIOANNOU G., MAVRIDIS P.: Generalized digital reassembly using geometric registration. In *Digital Heritage* (2015), vol. 2, pp. 549–556.
- [ASC*13] ARBACE L., SONNINO E., CALLIERI M., DELLEPIANE M., FABBRI M., IDELSON A. I., SCOPIGNO R.: Innovative uses of 3D digital technologies to assist the restoration of a fragmented terracotta statue. *J. of Cultural Heritage* 14, 4 (2013), 332 – 345.
- [Bal81] BALLARD D. H.: Generalizing the hough transform to detect arbitrary shapes. *Pattern recogn.* 13, 2 (1981), 111–122.
- [BCFS15] BIASOTTI S., CERRI A., FALCIDIENO B., SPAGNUOLO M.: 3D artifacts similarity based on the concurrent evaluation of heterogeneous properties. *J. Comput. Cult. Herit.* 8, 4 (2015), 19:1–19:19.
- [BDF*08] BIASOTTI S., DE FLORIANI L., FALCIDIENO B., FROSINI P., GIORGI D., LANDI C., PAPALEO L., SPAGNUOLO M.: Describing shapes by geometrical-topological properties of real functions. *ACM Computing Surveys* 40, 4 (2008), 1–87.
- [BMP13] BELTRAMETTI M., MASSONE A., PIANA M.: Hough transform of special classes of curves. *SIAM J. Imaging Sci.* 6, 1 (2013), 391–412.
- [BR12] BELTRAMETTI M. C., ROBBIANO L.: An algebraic approach to Hough transforms. *J. of Algebra* 37 (2012), 669–681.
- [DH72] DUDA R. O., HART P. E.: Use of the Hough transformation to detect lines and curves in pictures. *Commun. ACM* 15, 1 (1972), 11–15.
- [DIOHS08] DANIELS II J., OCHOTTA T., HA K. L., SILVA T. C.: Spline-based feature curves from point-sampled geometry. *The Visual Computer* 24, 6 (2008), 449–462.
- [EC15] EC: The Shape Repository. <http://visionair.ge.imati.cnr.it/ontologies/shapes/>, 2011–2015.
- [EK SX96] ESTER M., KRIEGEL H. P., SANDER J., XU X.: A density-based algorithm for discovering clusters in large spatial databases with noise. In *2nd Int. Conf. Knowledge Discovery and Data Mining* (1996), AAAI Press, pp. 226–231.

- [FBF77] FRIEDMAN J. H., BENTLEY J. L., FINKEL R. A.: An algorithm for finding best matches in logarithmic expected time. *ACM Trans. Math. Softw.* 3, 3 (1977), 209–226.
- [GWM01] GUMHOLD S., WANG X., MACLEOD R.: Feature extraction from point clouds. In *10th Int. Meshing Roundtable* (2001), pp. 293–305.
- [Ham] Virtual Hampson museum project. URL: <http://hampson.cast.uark.edu/>, <http://dx.doi.org/10.6067/XCV80G3MM0> doi: 10.6067/XCV80G3MM0.
- [Hou62] HOUGH P. V. C.: Method and means for recognizing complex patterns, 1962. US Patent 3,069,654.
- [HPW05] HILDEBRANDT K., POLTHIER K., WARDETZKY M.: Smooth feature lines on surface meshes. In *EG SGP* (2005), The Eurographics Association.
- [HT11] HARARY G., TAL A.: The Natural 3D Spiral. *Comput. Graph. Forum* (2011).
- [Ima] IMAGINARY - open mathematics. URL: <https://imaginary.org>.
- [IT11] ITSKOVICH A., TAL A.: Surface partial matching and application to archaeology. *Computers & Graphics* 35, 2 (2011), 334 – 341.
- [KDS10] KLEBER F., DIEM M., SABLATNIG R.: Proposing Features for the Reconstruction of Marble Plates of Ephesos. In *16th Int. Conf. on Virtual Systems and Multimedia* (2010), pp. 328–331.
- [KIST11] KOLOMENKIN M., ILAN SHIMSHONI I., TAL A.: Prominent field for shape processing of archaeological artifacts. *Int. J. Comput. Vision* 94, 1 (2011), 89–100.
- [KK06] KIM S.-K., KIM C.-H.: Finding ridges and valleys in a discrete surface using a modified mls approximation. *Comput. Aided Des.* 38, 2 (2006), 173–180.
- [Koe84] KOENDERINK J. J.: What does the occluding contour tell us about solid shape? *Perception* 13, 3 (1984), 321–330.
- [KST08] KOLOMENKIN M., SHIMSHONI I., TAL A.: Demarcating curves for shape illustration. *ACM Trans. Graph.* 27, 5 (2008), 157:1–157:9.
- [LBZ*13] LIU Z., BU S., ZHOU K., GAO S., HAN J., WU J.: A survey on partial retrieval of 3D shapes. *J. Comput. Sci. Technol.* 28, 5 (2013), 836–851.
- [LLZ10] LUO T., LI R., ZHA H.: 3D line drawing for archaeological illustration. *Int. J. Comput. Vision* 94, 1 (2010), 23–35.
- [MPCB15] MASSONE A. M., PERASSO A., CAMPI C., BELTRAMETTI M. C.: Profile detection in medical and astronomical images by means of the hough transform of special classes of curves. *J. Math. Imaging Vis.* 51 (2015), 269–310.

- [NDL11] NIGGEMANN E., DE DECKER J., LÉVY M.: The New Renaissance, 2011. Report of the “Comité des Sages” Reflection group on bringing Europe’s Cultural Heritage.
- [OBS04] OHTAKE Y., BELYAEV A., SEIDEL H.-P.: Ridge-valley lines on meshes via implicit surface fitting. *ACM Trans. Graph.* 23, 3 (2004), 609–612.
- [Pey] PEYRE G.: Toolbox graph - a toolbox to process graph and triangulated meshes. <http://www.ceremade.dauphine.fr/peyre/matlab/graph/content.html>.
- [PKG03] PAULY M., KEISER R., GROSS M.: Multi-scale feature extraction on point-sampled surfaces. *Comput. Graph. Forum* 22, 3 (2003), 281–289.
- [PPY*16] PINTUS R., PAL K., YANG Y., WEYRICH T., GOBBETTI E., RUSHMEIER H.: A survey of geometric analysis in cultural heritage. *Comput. Graph. Forum* 35, 1 (2016), 4–31.
- [Sha06] SHAMIR A.: Segmentation and Shape Extraction of 3D Boundary Meshes. Wyvill B., Wilkie A., (Eds.), Eurographics Association, pp. 137–149. Eurographics 06 STAR.
- [Shi95] SHIKIN E. V.: *Handbook and atlas of curves*. CRC, 1995.
- [SPS15] SAVELONAS M. A., PRATIKAKIS I., SFIKAS K.: Partial 3D object retrieval combining local shape descriptors with global fisher vectors.
- [SRT*14] SANTOS P., RITZ M., TAUSCH R., SCHMEDT H., MONROY R., STEFANO A. D., POSNIAK O., FUHRMANN C., FELLNER D. W.: Cult-Lab3D - On the Verge of 3D Mass Digitization. In *EG GCH* (2014), Klein R., Santos P., (Eds.).
- [STA] STARC repository. URL: <http://public.cyi.ac.cy/starcRepo/>.
- [SWRK11] SCHWARTZ C., WEINMANN M., RUITERS R., KLEIN R.: Integrated High-Quality Acquisition of Geometry and Appearance for Cultural Heritage. In *Int. Symp. on Virtual Reality, Archeology and Cultural Heritage* (2011), pp. 25–32.
- [TB14] TORRENTE M.-L., BELTRAMETTI M. C.: Almost vanishing polynomials and an application to the Hough transform. *J. of Algebra and Its Applications* 13, 08 (2014), 1450057.
- [TWW01] TANAKA J., WEISKOPF D., WILLIAMS P.: The role of color in high-level vision. *Trends in cognitive sciences* 5, 5 (2001), 211–215.
- [Vis] VISUAL COMPUTING LAB – ISTI – CNR: Meshlab. <http://meshlab.sourceforge.net/>.
- [WC08] WILLIS A. R., COOPER D. B.: Computational reconstruction of ancient artifacts: From ruins to relics. *IEEE Signal Processing Magazine* 25 (2008), 65–83.

- [YBYS08] YOSHIKAWA S., BELYAEV A., YOKOTA H., SEIDEL H.-P.: Fast, robust, and faithful methods for detecting crest lines on meshes. *Comput. Aided Geom. Des.* 25, 8 (2008), 545–560.

Recent titles from the IMATI-REPORT Series:

16-01: *Optimal strategies for a time-dependent harvesting problem*, G.M. Coclite, M. Garavello, L.V. Spinolo, February 2016.

16-02: *A new design for the implementation of isogeometric analysis in Octave and Matlab: GeoPDEs 3.0*, R. Vázquez, April 2016.

16-03: *Defect detection in nanostructures*, D. Carrera, F. Manganini, G. Boracchi, E. Lanzarone, April 2016.

16-04: *A study of the state of the art of process planning for additive manufacturing*, M. Livesu, M. Attene, M. Spagnuolo, B. Falcidieno, May 2016.

16-05: *Calcolo di descrittori ibridi geometria-colore per l'analisi di similarità di forme 3D*, A. Raffo, S. Biasotti, June 2016.

16-06: *An appointment scheduling framework to balance the production of blood bags from donation*, Seda Baş, Giuliana Carello, Ettore Lanzarone, Semih Yalçındağ, June 2016.

16-07: *From lesson learned to the refactoring of the DRIHM science gateway for hydro-meteorological research*, D. D'Agostino, E. Danovaro, A. Clematis, L. Roverelli, G. Zereik, A. Galizia, July 2016.

16-08: *Algorithms for the implementation of adaptive isogeometric methods using hierarchical splines*, E.M.Garau, R.Vázquez, July 2016.

16-09: *Feature curve identification in archaeological fragments using an extension of the Hough transform*, M.L. Torrente, S. Biasotti, B. Falcidieno, July 2016.

Istituto di Matematica Applicata e Tecnologie Informatiche "Enrico Magenes", CNR
Via Ferrata 5/a, 27100, Pavia, Italy

Genova Section: Via dei Marini, 6, 16149 Genova, Italy • **Milano Section:** Via E. Bassini, 15, 20133 Milano, Italy

<http://www.imati.cnr.it/>